Available online at www.sciencedirect.com
SCIENCE DIRECT®

Journal of the European Ceramic Society 24 (2004) 653–659

www.elsevier.com/locate/jeurceramsoc

Effects of powder preparation method on the microstructure and mechanical performance of ZTA/$LaAl_{11}O_{18}$ composites

Xihai Jin, Lian Gao*

The State Key Lab of High Performance Ceramics and Superfine Microstructure, Shanghai Institute of Ceramics, Chinese Academy of Sciences, Shanghai 200050, PR China

Received 28 October 2002; received in revised form 18 March 2003; accepted 6 April 2003

Abstract

ZTA/$LaAl_{11}O_{18}$ (ZAL) composites were prepared by two different methods, and were denoted as ZAL-F and ZAL-C, respectively. In both of the materials, ZrO_2 was exclusively in tetragonal symmetry and did not transform to m-ZrO_2 after the fracture of the samples. TEM, SAED and HRTEM observations indicated that the $LaAl_{11}O_{18}$ grains took a platelet-like morphology, with their main surface planes parallel to the (001) plane. The ZAL-F sample showed a higher sintering ability, more homogeneous microstructure and finer Al_2O_3 grains than ZAL-C. And owing to the higher grain boundary strength in ZAL-F, the Al_2O_3 grains there showed a higher propensity to transgranular fracture than those in ZAL-C. The strength of ZAL-F was about 1 GPa, almost 20% higher than that of ZAL-C, although their toughness was very close.

Keywords: Composites; ZrO_2; $LaAl_{11}O_{18}$; ZTA; Platelets; Mechanical properties

1. Introduction

The combinative reinforcing effect of multiple reinforcing agents has been actively used in the material design of ceramic composites.[1–3] P. F. Becher found that ZrO_2 and SiC whisker showed a synergetic toughening effect to mullite.[1] Nakahira reported that the strength of an Al_2O_3/5 vol.%SiC nanocomposite was increased from 1050 MPa to 1700 MPa after the addition of 20 vol.% 3Y-TZP.[2] While Kanamaru reported that the strength of an Al_2O_3/20 wt.%SiC whisker composite was increased from 700 to 1200 MPa after the addition of 4 wt.% TiC nanoparticles.[3] However, despite the great successes in the mechanical property improvements of these materials, there were difficulties in sintering and homogeneously dispersing the nanoparticles and whiskers in these composites, which restricted the commercialization of these materials.

Recently, readily sinterable Al_2O_3 composites with in-situ formed aluminate platelets or elongated particles have been reported.[4] Among them, the Al_2O_3/$LaAl_{11}O_{18}$ composite was especially attractive and has been widely studied,[5–8] because of its high mechanical performances. ZrO_2 showed a good chemical compatibility with both Al_2O_3 and $LaAl_{11}O_{18}$, and could be used as a second reinforcing agent in the Al_2O_3/$LaAl_{11}O_{18}$ composite to realize a combinative reinforcement of Al_2O_3 by ZrO_2 and $LaAl_{11}O_{18}$.

In this work, ZTA/$LaAl_{11}O_{18}$ composites containing 10 vol.% 2Y–ZrO_2 and 20 vol.% $LaAl_{11}O_{18}$ were prepared, the microstructures and mechanical properties of these composites were investigated.

2. Experimental procedure

2.1. Powder preparation

Two different methods were adopted in preparing the ZTA/$LaAl_{11}O_{18}$ (ZAL) powders, and the resulting materials were denoted as ZAL-C and ZAL-F, respectively. During the powder preparation of ZAL-F, α-Al_2O_3 (HFF-5, Wusong Chemical Fertilizer Factory, 0.3 μm) was dispersed in distilled water using 2 wt.% NH_4-PAA dispersant. Then $ZrOCl_2$, $La(NO_3)_3$, $Al(NO_3)_3$ and $Y(NO_3)_3$ mixing solution and 4 N ammoniated water

* Corresponding author. Tel.: +86-21-52412718; fax: +86-21-52413122.
E-mail address: liangaoc@online.sh.cn (L. Gao).

0955-2219/03/$ - see front matter © 2003 Elsevier Ltd. All rights reserved.
doi:10.1016/S0955-2219(03)00257-7

were added simultaneously into the Al_2O_3 suspension under vigorous stirring. The quantities of $Al(NO_3)_3$ and $La(NO_3)_3$ were exactly the same as that needed to form $LaAl_{11}O_{18}$. After the precipitation process was finished, the mixture suspension was adjusted to pH 9 and aged for 1–2 h. The resulting precipitate was collected by vacuum filtering and washed successively with distilled water and hot ethanol for 5 and 2 times, respectively. Finally the precipitate was dried at 100 °C overnight and subsequently calcined at 800 °C for 1 h.

ZAL-C powder was prepared by nearly the same experimental procedure as ZAL-F, except some difference in the starting materials of Al_2O_3. α-Al_2O_3 (HFF-5, Wusong Chemical Fertilizer Factory, 0.3 μm) was used as the only source of Al_2O_3 in ZAL-C powder, and no $Al(NO_3)_3$ was used.

2.2. Sintering and characterization

Sintering was conducted by hot-pressing in an argon atmosphere under a pressure of 30 MPa at temperatures from 1300 to 1500 °C for 1 h. The sintered samples were machined and cut into beams measuring 35×5×2.5 mm. The tensile surfaces and long edges of the beams were polished and beveled for strength testing.

The density and phase assembly of the samples were measured by the water-displacement method and X-ray diffractometry (XRD; Model D/MaX rB, Rigaku Co., Ltd., Tokyo, Japan), respectively. The strength was tested using a three-point-bend testing machine (Model 1195, Instron Corp., Danvers, MA), with a gauge length of 30 mm and a cross-head speed of 0.5 mm/min. The toughness was determined by the Vickers indentation method, with a load of 10 kg and a dwell time of 10 s, using the empirical equation given by Anstis et al.[9] Scanning electron microscopy (SEM; Model JSM-6700F, JEOL, Tokyo, Japan) and transmission electron microscopy (TEM; Model 2010CX, JEOL) were used to examine the microstructure of the samples.

3. Results and discussions

3.1. Sintering

The sintering behaviors of ZAL-C and ZAL-F composites were investigated and shown in Fig. 1. Although both samples only could be fully densified at 1400 °C or above, the ZAL-F sample showed a much higher density than ZAL-C when the sintering temperature was below 1400 °C, because of the difference in the powder characteristics of ZAL-F and ZAL-C. In addition to the fine ZrO_2 and La_2O_3 particles as contained in ZAL-C powder, additional fine Al_2O_3 particles (~20 vol.%) derived from $Al(NO_3)_3$ were contained in ZAL-F powder. In the initial period of hot pressing, the ZAL-F

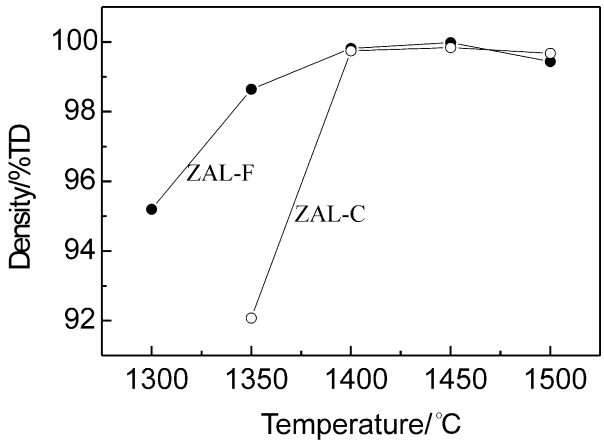

Fig. 1. The densities of ZAL-C and ZAL-F as a function of sintering temperature.

powder could be packed more densely than ZAL-C powder through particle rearrangement, therein ZrO_2, La_2O_3 and the fine Al_2O_3 particles filled into the interstices among coarse α-Al_2O_3 particles. While in ZAL-C powder, the interstices between coarse α-Al_2O_3 particles could not be filled as effectively as in ZAL-F, because of the low content of fine particles there. The improved the packing behavior of ZAL-F powder partially accounted for the lower sintering temperature, as found by Helling and Shi etc.[10,11] Secondly, due to the high sinterability of the fine Al_2O_3 particles, the ZAL-F powder should be more sintering active than the ZAL-C powder. This could also lead to a decrease in the sintering temperature of ZAL-F.

3.2. Phase assemblage

The XRD patterns of ZAL-C and ZAL-F sintered at 1400 and 1500 °C are shown in Fig. 2. All the samples showed almost identical XRD patterns, where only reflections characterized to Al_2O_3, $LaAl_{11}O_{18}$ and t-ZrO_2 were observed, no other crystalline phases were detected.

Cinibulk prepared $LaAl_{11}O_{18}$ by a sol-gel method, found that only ~85% of $LaAl_{11}O_{18}$ was formed after calcining a La_2O_3–Al_2O_3 gel at 1450 °C for 2 h.[12] Jantzen also reported that it was difficult to obtain phase-pure $LaAl_{11}O_{18}$ even after heating an $Al(OH)_3$–$La(NO_3)_3{\cdot}6H_2O$ mixture at 1650 °C for 115 h.[13] However, Carmen found that La_2O_3 was completely converted to $LaAl_{11}O_{18}$ by calcining a La_2O_3–Al_2O_3 gel at 1300 °C for 5 h.[8] While in the present experiment, La_2O_3 was also completely converted to $LaAl_{11}O_{18}$ at a temperature no higher than 1400 °C. It seemed that the crystallizing behaviors of $LaAl_{11}O_{18}$ could be very different, even if the Al_2O_3–La_2O_3 powders were prepared by quite similar methods. In the Al_2O_3–La_2O_3 powders prepared by Cinibulk and Jantzen, the mole ratio of Al_2O_3 to La_2O_3 was the same as that in $LaAl_{11}O_{18}$,

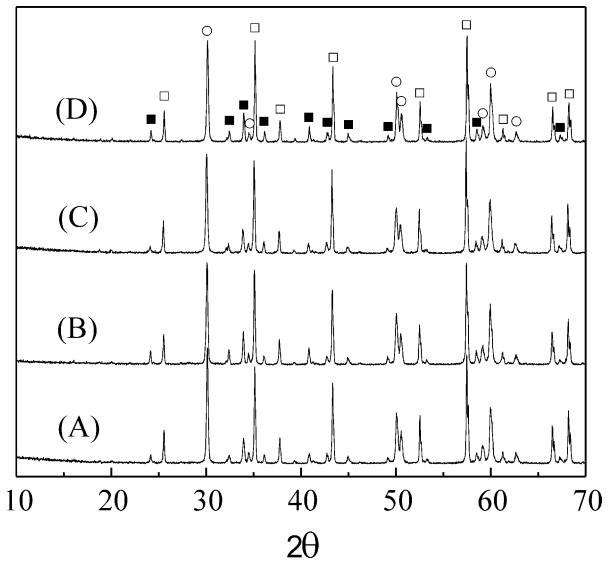

Fig. 2. XRD patterns of ZAL-C and ZAL-F sintered at different temperatures, where the circles represent t-ZrO_2, the solid and hollow squares represent $LaAl_{11}O_{18}$ and α-Al_2O_3, respectively. (A) ZAL-F, 1400 °C; (B) ZAL-F, 1500 °C; (C) ZAL-C, 1400 °C; (D) ZAL-C, 1500 °C.

whereas in the present ZAL systems and the Al_2O_3–La_2O_3 gel prepared by Carmen, the mole ratio of Al_2O_3 to La_2O_3 was much higher. This suggested that the excessive Al_2O_3 might have taken certain effect in promoting the formation of $LaAl_{11}O_{18}$ by shifting the $LaAl_{11}O_{18}$ formation reaction towards right side.

3.3. Microstructure and fracture behavior

Fig. 3 shows the back-scattered SEM images of the polished surfaces of ZAL-C and ZAL-F sintered at 1400 and 1500 °C. According to the difference in grain contrast, three kinds of grains were observed in the samples sintered at 1500 °C. The dark gray one was Al_2O_3, the light gray one $LaAl_{11}O_{18}$ and the bright one t-ZrO_2. It was difficult to distinguish $LaAl_{11}O_{18}$ from Al_2O_3 and t-ZrO_2 in the samples sintered at 1400 °C, because of the small grain size of $LaAl_{11}O_{18}$ and its intermediate contrast, which made them merge into the background. In comparison with ZAL-C, the phase distribution in ZAL-F was more homogeneous. In ZAL-C, local areas highly concentrated with ZrO_2 and $LaAl_{11}O_{18}$ grains were frequently observed while such areas were seldom observed in ZAL-F.

Fig. 4 shows the SEM micrographs of the thermally etched surfaces of ZAL-F and ZAL-C samples. The Al_2O_3 grains in ZAL-F were relatively finer and more uniform. For the samples sintered at 1400 and 1500 °C, the average grain sizes of Al_2O_3 were about 0.4 μm and 0.8 μm in ZAL-F, and were about 0.45 and 0.9 μm in ZAL-C, respectively. $LaAl_{11}O_{18}$ grains generally took an elongated morphology in both ZALF and ZAL-C. $LaAl_{11}O_{18}$ grains in ZAL-F sintered at 1400 °C showed a thickness of 50 nm and length of 400 nm, and were sandwiched between Al_2O_3 grains. While under the same sintering conditions, the $LaAl_{11}O_{18}$ grains in ZAL-C were much larger, their thickness and length were about 200 and 600 nm in average. As the sintering temperature was increased to 1500 °C, the $LaAl_{11}O_{18}$ grain sizes for both samples became comparable, which were about 0.5 μm in thickness and 1.5–2.0 μm in length.

Fig. 5 shows the SEM micrographs of the fracture surfaces of ZAL-C and ZAL-F. The ZAL-F sample showed a much flatter fracture surface than ZAL-C, and a large number of Al_2O_3 and $LaAl_{11}O_{18}$ grains in ZAL-F were broken transgranularly. While in ZAL-C, more Al_2O_3 and $LaAl_{11}O_{18}$ grains showed an intergranular fracture feature with significant grain pull out.

The origins of the differences in the microstructure and fracture behaviors of ZAL-F and ZAL-C can be traced back to the powder preparing processes. In the starting materials of ZAL-F powder, part of α-Al_2O_3 was replaced with $Al(NO_3)_3$. During the subsequent precipitation process, $Zr(OH)_4$ and $La(OH)_3$ precipitated together with $Al(OH)_3$, which enabled an intimate mixing of ZrO_2 and La_2O_3 with Al_2O_3 in the final powder and a homogeneous phase distribution in the sintered sample. The formation of finer and more uniform Al_2O_3 grains in ZAL-F was resulted from the pinning effect of ZrO_2 and $LaAl_{11}O_{18}$ on Al_2O_3 grain growth.[5,8,14,15] Because although both ZAL-F and ZAL-C contained the same amount of ZrO_2 and $LaAl_{11}O_{18}$, the ZrO_2 and $LaAl_{11}O_{18}$ grains in ZAL-F showed a stronger pinning effect on Al_2O_3 grain growth than their counterparts in ZAL-C, due to the more homogeneous phase distribution in ZAL-F.

The fine Al_2O_3 particles derived from $Al(NO_3)_3$ in ZAL-F powder showed a higher reactivity and were more liable to form $LaAl_{11}O_{18}$ with La_2O_3 than the coarse α-Al_2O_3 particles. While in ZAL-C, $LaAl_{11}O_{18}$ could only be formed between La_2O_3 and the coarse α-Al_2O_3. This led to the formation of finer $LaAl_{11}O_{18}$ grains in ZAL-F sintered at 1400 °C, when the sintering temperature was not much above the formation temperature of $LaAl_{11}O_{18}$ (~1300 °C). As the sintering temperature was increased to 1500 °C, a temperature much higher than the $LaAl_{11}O_{18}$ formation temperature, $LaAl_{11}O_{18}$ grains in both samples underwent extensive grain growth. As a result, the grain sizes of $LaAl_{11}O_{18}$ in them became comparable.

Due to the thermal expansion coefficient difference between ZrO_2 (10.5×10^{-6}/°C) and Al_2O_3 (8.5×10^{-6}/°C), a compressive thermal stress was imposed on Al_2O_3 grain boundaries after sintering, resulting in an increased Al_2O_3 grain boundary strength. However, due to the more homogeneous distribution of ZrO_2 in ZAL-F, such grain boundary strengthening effect was more pronounced in ZAL-F than that in ZAL-C. As a result,

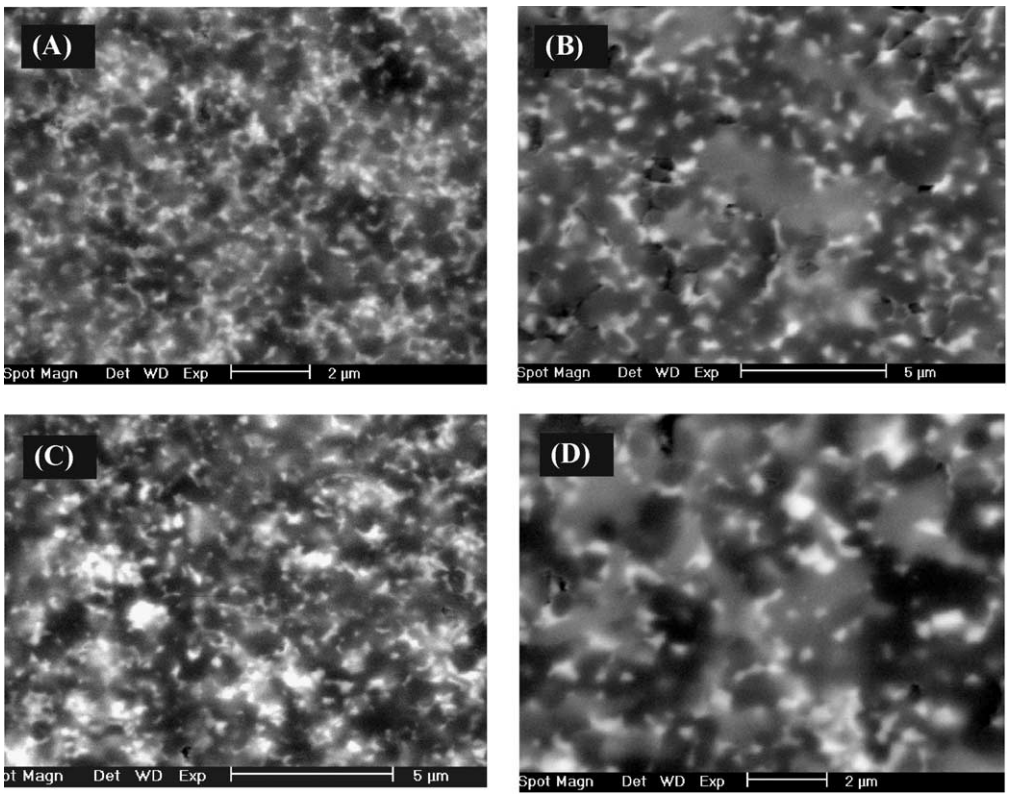

Fig. 3. The back scattered SEM micrographs of the polished surfaces of ZAL-C and ZAL-F sintered at different temperatures: (A) ZAL-F, 1400 °C; (B) ZAL-F, 1500 °C; (C) ZAL-C, 1400 °C; (D) ZAL-C, 1500 °C.

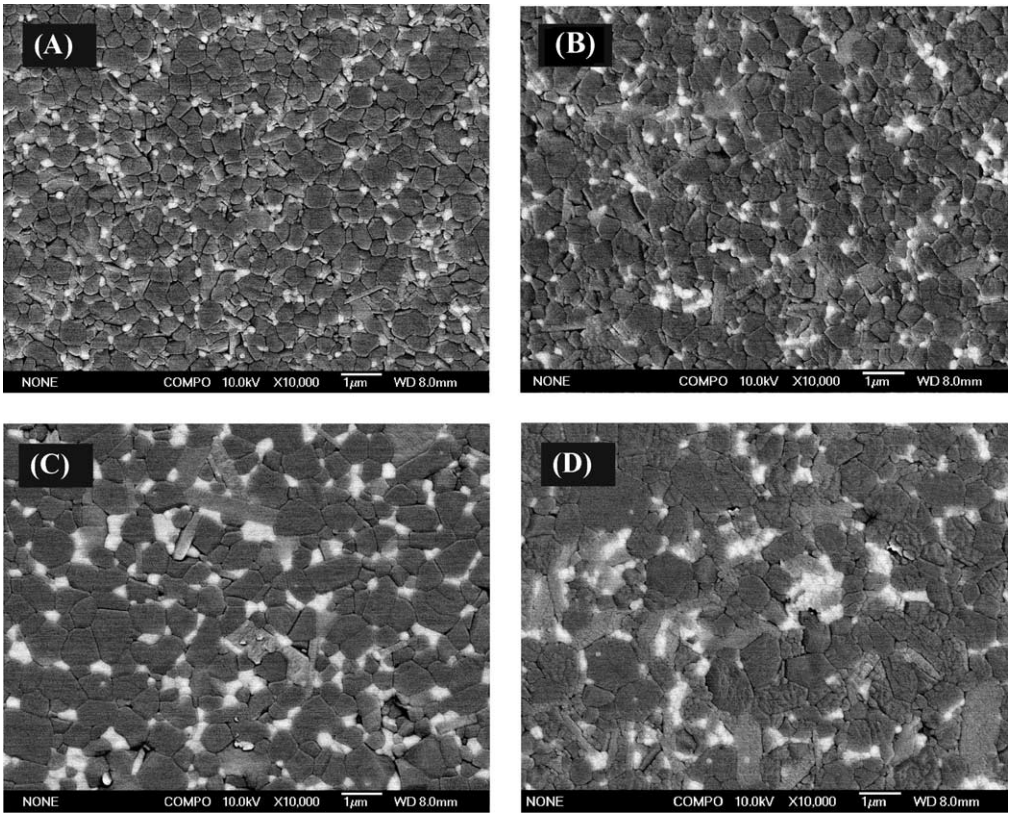

Fig. 4. The back scattered SEM micrographs of the thermally etched surfaces of ZAL-C and ZAL-F sintered at different temperatures: (A) ZAL-F, 1400 °C; (B) ZAL-F, 1500 °C; (C) ZAL-C, 1400 °C; (D) ZAL-C, 1500 °C.

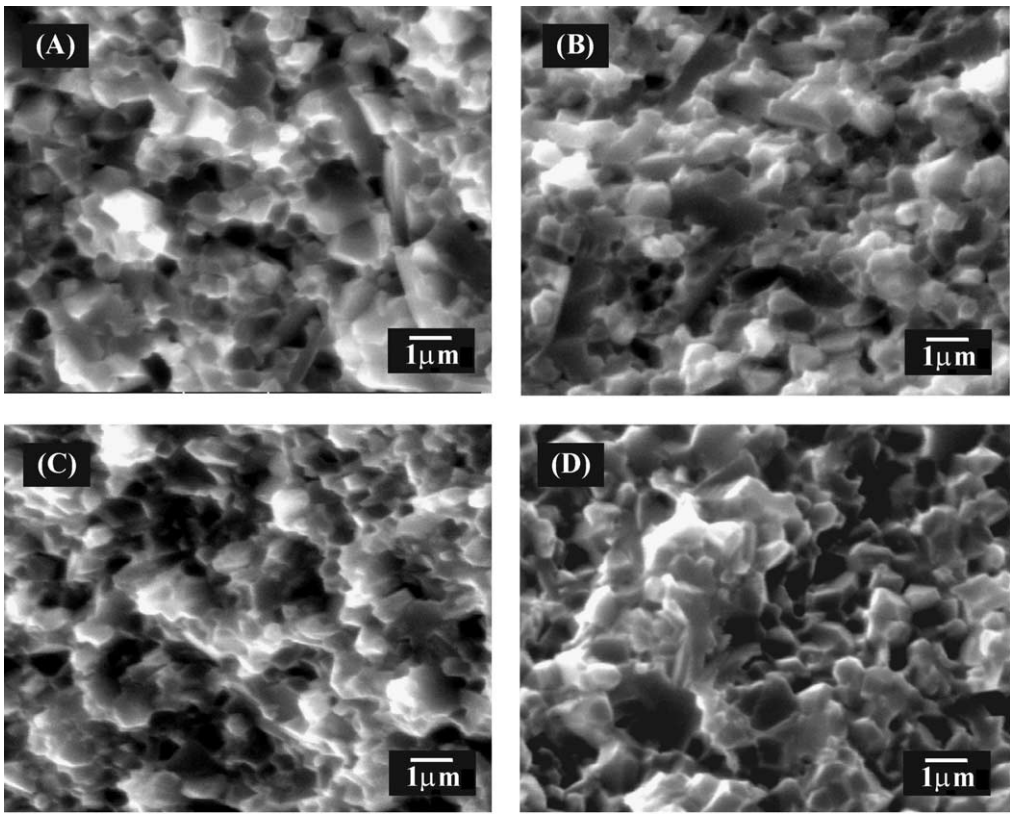

Fig. 5. SEM micrographs showing the fracture surfaces of ZAL-C and ZAL-F sintered at different temperatures: (A) ZAL-F, 1450 °C; (B) ZAL-F, 1500 °C; (C) ZAL-C, 1450 °C; (D) ZAL-C, 1500 °C.

the Al_2O_3 grains in ZAL-F were more liable to transgranular fracture than those in ZAL-C.

3.4. Grain shape and orientation of $LaAl_{11}O_{18}$

$LaAl_{11}O_{18}$ grains mainly showed an anisometric morphology, as observed in the SEM micrographs of both ZAL-C and ZAL-F. However, up to now, there is still much controversy about the exact shape of $LaAl_{11}O_{18}$ grains. Carmen suggested that $LaAl_{11}O_{18}$ grains took a platelet-like shape,[8] while Fujii claimed that $LaAl_{11}O_{18}$ grains were needle-like.[16] In order to clarify the problem, TEM and HRTEM (high resolution transmission electron microscopy) were conducted on the ZAL-F sample sintered at 1500 °C, as shown in Figs. 6 and 7. Two kinds of $LaAl_{11}O_{18}$ grains were generally observed in the sample, "equiaxed" ones and "elongated" ones. The diameters of the "equiaxed" $LaAl_{11}O_{18}$ grains were similar to the lengths but much larger than the thickness of the "elongated" $LaAl_{11}O_{18}$ grains. The SAED (selected area electron diffraction) patterns and the HRTEM image of the "elongated" grains indicated that they were oriented perpendicular to the [001] direction and parallel to the (001) planes.

According to the theory of crystallography,[17] a naturally growing prism-like (or elongated) crystal should be bounded by a set of symmetry-equivalent faces parallel to a common axis. $LaAl_{11}O_{18}$ shows a hexagonal lattice symmetry, and [001] axis is the only high order symmetry axis (sixfold) in it. Thus if the $LaAl_{11}O_{18}$ grains took a needle-like shape, it is more likely to orient in rather than perpendicular to the [001] direction as found in the needle-like β-Si_3N_4 grains. Therefore, the chance of forming a needle-like $LaAl_{11}O_{18}$ grain was small. In fact, All the TEM, HRTEM and SAED evidences point to a platelet-like $LaAl_{11}O_{18}$ grain.

If a crystal took a platelet-like shape (pinacoid), its main surface planes (i.e. the large surface planes) should be symmetry-equivalent and parallel to each other.[17] The {00l} plane group of a $LaAl_{11}O_{18}$ crystal has the fewest number (i.e. two) of symmetry-equivalent planes, thus the (001) and $(00\bar{1})$ planes were the most suitable candidates for the main surface planes of the platelet-like $LaAl_{11}O_{18}$ grain. The good agreement between the theoretical prediction and the experimental results indicated that the $LaAl_{11}O_{18}$ grains should be platelet-like. The "equiaxed" and the "elongated" $LaAl_{11}O_{18}$ grains observed under TEM were just the different cross-sections of platelet-like $LaAl_{11}O_{18}$ grains.

3.5. Mechanical properties

Table 1 lists the mechanical properties of ZAL-C and ZAL-F sintered at 1400–1500 °C. Both of the materials

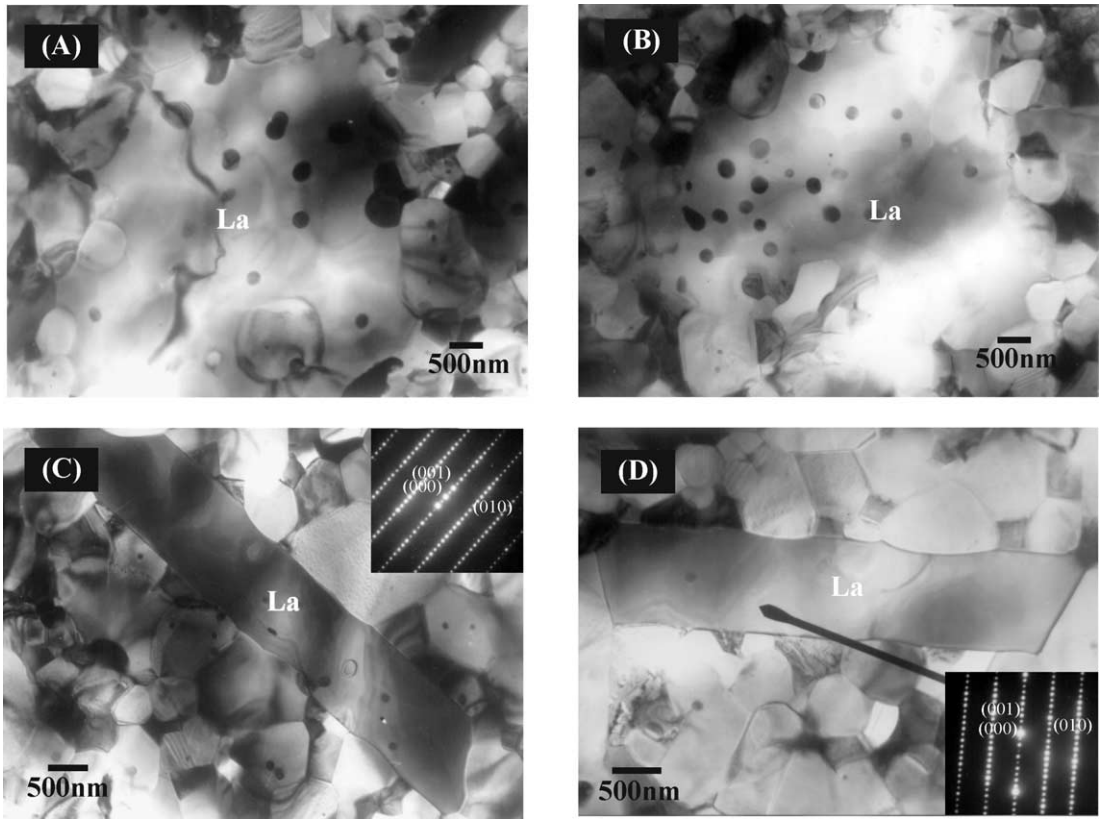

Fig. 6. The TEM images of ZAL-F sintered at 1500 °C, where La represent $LaAl_{11}O_{18}$ grains.

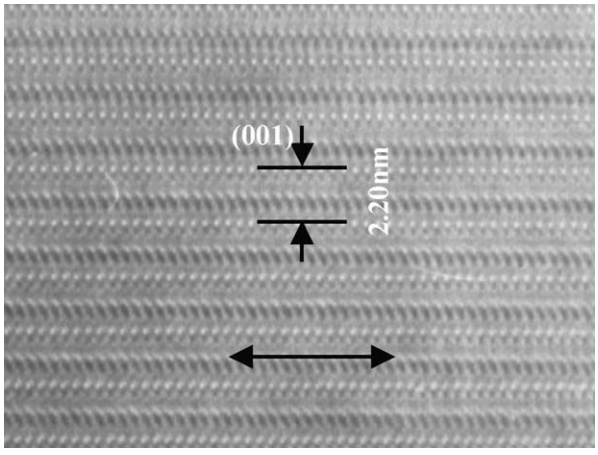

Fig. 7. The HRTEM image of the "elongated" $LaAl_{11}O_{18}$ grain shown in Fig. 6 (D), where the double-ended arrow indicates the grain orientation of the $LaAl_{11}O_{18}$ grain.

showed considerably higher strengths than the conventional single-phase Al_2O_3 (~500 MPa), although their toughness was comparable to that of the latter. The formation of finer and more uniform microstructures in the ZAL samples, due to the pinning effects of ZrO_2 and $LaAl_{11}O_{18}$ on Al_2O_3 grain growth, was the most important reason for their strength improvement. Furthermore, the strengthened grain boundaries by the thermal stress in ZAL samples was likely another factor accounting for their high strengths.

Table 1
The mechanical properties of ZAL-F and ZAL-C sintered at different temperatures

	Sintering temperature (°C)	Strength (MPa)	Toughness ($MPa \cdot m^{1/2}$)
ZAL-C	1400	806	3.2
	1450	852	3.7
	1500	794	3.4
ZAL-F	1400	950	3.4
	1450	1020	3.8
	1500	1000	3.8

XRD conducted on the fracture surfaces of the ZAL samples found that the t-ZrO_2 in both ZAL-F and ZAL-C was too stable to transform to m-ZrO_2 after the failure of the materials, because of the combinative stabilization of t-ZrO_2 by Y_2O_3 and La_2O_3.[18] The poor transformability of t-ZrO_2 should be one of the most important reasons accounting for the low toughness of the present materials. In addition, owing to the intrinsic weakness of $LaAl_{11}O_{18}$, although the $LaAl_{11}O_{18}$ platelets were able to toughen the matrix to some extent, this toughening effect was relatively weak compared with that of the coarse grained Al_2O_3. This also limited the toughness increase of the ZAL materials.

Finally, it can be seen from Table 1, that although the toughness of ZAL-F and ZAL-C was very close, the

strength of ZAL-F was about 20% higher than that of ZAL-C, mainly because of the more uniform microstructure and the stronger grain boundary in ZAL-F.

4. Conclusions

1. Because of the partial replacement of coarse α-Al_2O_3 with fine Al_2O_3 derived from $Al(NO_3)_3$ in the ZAL-F powder and the high sinterability of the fine Al_2O_3 particles, ZAL-F showed a better sinterability than ZAL-C.
2. ZrO_2 grains in both ZAL-F and ZAL-C were totally in tetragonal symmetry; these t-ZrO_2 grains were untransformable under the fracture stress, restricting the toughness improvement of the materials.
3. ZAL-F showed a relatively finer and more uniform microstructure than ZAL-C. The more intimate mixing of the chemical ingredients in the ZAL-F powder and the stronger pinning effect of ZrO_2 and $LaAl_{11}O_{18}$ on Al_2O_3 grain growth in ZAL-F were thought to be responsible for such differences between the microstructures of the two materials.
4. Al_2O_3 grains in ZAL-F showed a higher propensity to transgranular fracture than those in ZAL-C, due to the stronger grain boundary strengthening effect of ZrO_2 in it.
5. ZAL-F showed a higher strength than ZAL-C, mainly because of the formation of a more homogeneous microstructure and the stronger grain boundary in the former material.
6. $LaAl_{11}O_{18}$ grains took a platelet-like morphology, with their main surface planes parallel to the (001) planes.

References

1. Becher, P. F. and Tiegs, T. N., Toughening behavior involving multiple mechanisms: whisker reinforcement and Zirconia toughening. *J. Am. Ceram. Soc.*, 1987, **70**(9), 651–654.
2. Nakahira, A., Fukushima, Y. and Niihara, K., The Al_2O_3–SiC–ZrO_2 composites. *Powder and powder metallurgy (Japan)*, 1989, **36**(4), 746–751.
3. Kanamaru, M., Tatsuno, T. and Kusaka, T., Hot-pressed Al_2O_3/SiC whisker/TiC nano-composites. *J. Ceram. Soc. Jpn.*, 1992, **100**(4), 408–412.
4. Chen, P.-L. and Chen, I.-W., In-situ alumina/aluminate platelet composites. *J. Am. Ceram. Soc.*, 1992, **75**(9), 2610–2612.
5. Yasuoka, M., Hirao, K., Brito, M. E. and Kanzaki, S., High-strength and high-fracture-toughness ceramics in the Al_2O_3/$LaAl_{11}O_{18}$ systems. *J. Am. Ceram. Soc.*, 1995, **78**(7), 1853–1856.
6. Jang, B.-K. and Kishi, T., Fabrication and microstructure of Al_2O_3 matrix composites by in-situ reaction in the Al_2O_3–La_2O_3 system. *J. Ceram. Soc. Jpn.*, 1998, **106**(8), 739–743.
7. Yasuoka, M., Hirao, K., Brito, M. E. and Kanzaki, S., Microstructure and mechanical properties of alumina based ceramics with changed amounts of β-lanthanaluminate. *J. Ceram. Soc. Jpn.*, 1997, **105**(8), 641–644.
8. Solano, C. B., Esquivias, L. and Messing, G. L., Effect of preparation conditions on phase formation, densification, and microstructure evolution in La–β–Al_2O_3/Al_2O_3 composites. *J. Am. Ceram. Soc.*, 1999, **82**(5), 1318–1324.
9. Anstis, G. R., Chantikul, P., Lawn, B. R. and Marshall, D. B., A critical evaluation of indentation techniques for measuring fracture toughness: I, direct crack measurement. *J. Am. Ceram. Soc.*, 1981, **64**(3), 533–535.
10. Helling, R. J. and Ferkel, H., Using nanoscaled powder as an additive in coarse-grained powder. *J. Am. Ceram. Soc.*, 2001, **84**(2), 261–266.
11. Shi, J.-L. and Zhang, J. D., Compaction and sintering behavior of bimodal alumina powder suspensions by pressure filtration. *J. Am. Ceram. Soc.*, 2000, **83**(4), 737–742.
12. Cinibulk, M. K., Synthesis and characterization of sol-gel derived lanthanum hexaluminate powders and films. *J. Mater. Res.*, 1995, **10**(1), 71–76.
13. *Powder Diffraction File*, International Center for Diffraction Data, Newtown Square, PA, 1983, Card No. 34-467.
14. Taruta, S., Kawashima, K., Kitajima, K., Takusagawa, X., Okada, N. K. and Otsuka, N., Influence of ZrO_2 addition on the sintering behavior of bimodal size distributed alumina powder mixtures. *J. Ceram. Soc. Jpn*, 1994, **102**(2), 139–144.
15. Lange, F. F., Yamaguchi, T., Davis, B. I. and Morgan, P. E. D., Effect of ZrO_2 inclusions on the sinterability of Al_2O_3. *J. Am. Ceram. Soc.*, 1988, **71**(6), 446–448.
16. Fujii, T., Muragaki, H. and Hirano, H. In *Ceramics Transaction, vol. 22: Ceramic Powder Science IV*, ed. S. Hirano, G. L. Messing and H. Hausner. American Ceramic Society, Westerville, OH, 1991, pp. 693–698.
17. Giacovazzo, C., Monaco, H. L., Viterbo, D., Scordari, F., Gilli, G., Zanotti, G. and Catti, M., *Fundamentals of Crystallography, International Union of Crystallography*, Oxford University Press, pp. 15.
18. Bastide, B., Odier, P. and Coutures, J. P., Phase equilibrium and martensitic transformation in lanthana-doped zirconia. *J. Am. Ceram. Soc.*, 1988, **71**(6), 449–453.